PSFC/RR-08-4

Millimeter-Wave Measurements of High Level and Low Level Activity Glass Melts

Final Report

Paul P. Woskov, S. K. Sundaram *, and William E. Daniel, Jr.**

* Pacific Northwest National Laboratory
** Savannah River National Laboratory

May 2008

Plasma Science and Fusion Center
Massachusetts Institute of Technology
Cambridge MA 02139 USA

This work was supported by the U.S. Department of Energy, Grant No. DE-FG02-05ER63978. Reproduction, translation, publication, use and disposal, in whole or in part, by or for the United States government is permitted.

Millimeter-Wave Measurements of High Level and Low Level Activity Glass Melts

(Finial Report 2008)
DE-FG02-05ER63978

Principal Investigators

Dr. Paul P. Woskov
Massachusetts Institute of Technology
Plasma Science and Fusion Center
NW16-110
167 Albany Street
Cambridge, MA 02139
617-253-8648
617-253-0700 (fax)
ppw@psfc.mit.edu

Dr. S. K. Sundaram
Pacific Northwest National Laboratory
P.O. Box 999 / MS K6-24
Richland, WA 999352
509-373-6666
509-376-3108 (fax)
sk.sundaram@pnl.gov

Dr. William E. Daniel, Jr.
Savannah River National Laboratory
Building 999-W
Aiken, SC 29808
803-819-8463
803-819-8416 (fax)
gene.daniel@srnl.gov

1. Introduction

Nuclear waste vitrification melters currently lack sophisticated on-line monitoring capability to ensure efficient operation and to guarantee in real time the production of a high quality glass waste product that meets stringent regulatory and disposal requirements. This lack of on-line monitoring capability is of particular concern for the costly multi-decade national effort in the U. S. to clean up cold war legacy waste, where the waste streams have complex chemistry and are not well characterized. Current operations at the Defense Waste Processing Facility (DWPF) at the Savannah River Site and future operations at the Waste Treatment Plant (WTP), now under construction at Hanford, rely on predictive models for vitrification because of the lack of on-line monitoring of most melter processing parameters. This necessitates conservative operation to take into account uncertainties in the modeling and the ability to control actual input parameters. It also makes the operations susceptible to unpredictable anomalies such as foaming, liquidus crystallization, noble metals build up, and salt layer formation. Predictive modeling will become increasingly more difficult in time as the waste glass chemistry evolves with changes in the waste feed compositions. Additionally, the predictive models are limited by experimental validation, thus building more conservatism into the models. Comprehensive on-line real time monitoring of the vitrification process would lessen the uncertainties, improve processing efficiencies (by measuring directly inside a melter any deviations in a property (e.g., viscosity) from property model implanted and helping improvement of the model leading to high efficiencies and throughput), and help safeguard the facilities from anomalies. Advanced high temperature thermal analytical tools could also address the needs identified at the Hanford site and at the Savannah River Site (SRS) for increased waste loading and accelerated cleanup.

Much of the desired on-line monitoring capabilities can be realized through the use of millimeter-wave (MMW) technologies. Electromagnetic radiation in the 10 – 0.3 mm (30 – 1000 GHz) range of the spectrum is ideally suited for remote measurements in harsh, optically unclean, industrial, and unstable processing environments. Millimeter waves are long enough to penetrate optical/infrared obscured viewing paths through dust, smoke, and debris, but short enough to provide spatially resolved point measurements for profile information. Another important advantage is the ability to fabricate efficient MMW melter viewing components from refractory materials because optical or infrared quality is not required in the millimeter-wave wavelength range. The same ceramics and alloys from which the melter is constructed can be used to fabricate MMW waveguide/mirror components that go into the melter for long life survivability.

MMW techniques and technologies offer new robust diagnostic tools for glass melt monitoring in a high temperature and radioactive melter environment that other technologies can not access. These new tools should also make possible new insights into the dynamics of molten glass science and into nuclear waste glass melt property modeling because of the new way the melt properties are measured. In addition, these new monitoring developments contribute toward modernizing nuclear waste glass vitrification operations to industrial standards of feed-back control as employed by most

industries in manufacturing. The goal of more fully monitoring a melter is illustrated in Figure 1, where a cross-section of the DWPF melter is shown with the desired on-line diagnostics that would improve melter control. Currently, none of these listed measurements are being made in real-time on present production nuclear waste glass melters. However, many of these desired monitoring capabilities have now been demonstrated with the MMW techniques described here. The new MMW monitoring capabilities that have been demonstrated include those for melt viscosity, emissivity, temperature, foaming, salt layer formation, and cold cap temperature mapping. These developments have been accomplished both in the laboratory and in engineering scale test melters. Other monitoring capabilities that have not yet been demonstrated such as liquidus formation and noble metals accumulation have the potential to be developed based on this work. Consequently, the vision of a well-instrumented melter with a feed-back control illustrated in Figure 1 has the potential of becoming a reality with these new developments.

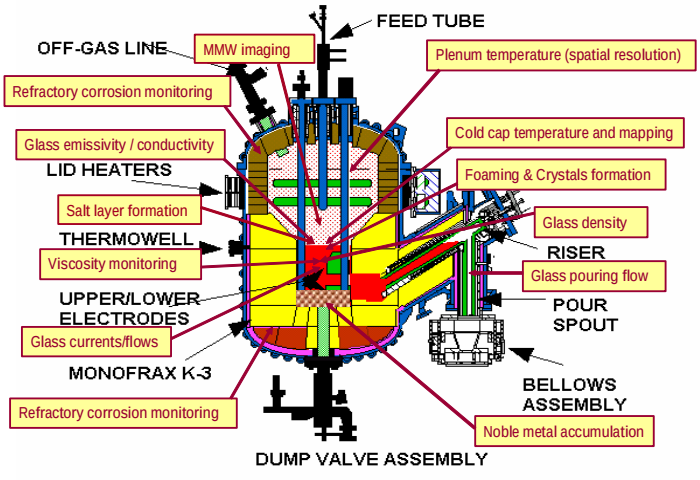

Figure 1. Long range objective to modernize nuclear waste glass melters with on-line monitoring.

2. Improving Melter Operation and Throughput

2.1. Melter Control

The Defense Waste Processing Facility at the Savannah River Site uses a feed-forward system to control the glass properties in the melter to ensure the vitrified waste satisfies waste acceptance protocols for long term storage and disposal as well as process operating constraints. The feed-forward system uses Statistical Process Control techniques where glass properties and their associated processing constraints are predicted using empirical models based on waste feed compositions, mostly validated by laboratory testing with limited research-scale melter testing. Due to this conservative approach, acceptable glasses with higher waste loadings can be rejected because the glass property (liquidus, durability, viscosity) is indeterminate (i.e., the applicability of the model is not certain). This type of feed-forward model predictive control is necessary since there are no reliable on-line glass property measurement devices. With online glass property measurement devices a more traditional feedback control system could be used like shown in Figure 2. Feedback control is the industrial standard employed by more companies due to its ability to maintain control despite unknown disturbances.

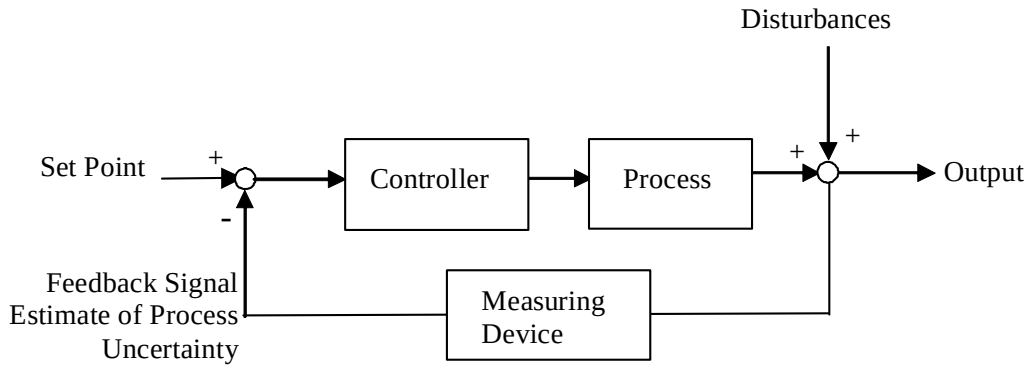

Figure 2. Classic Feedback Control Scheme

For high temperature melters that vitrify radioactive wastes like the ones used at DWPF at SRS and at the West Valley Demonstration Project (WVDP) and the ones planned for the River Protection Project at Hanford, there are no reliable glass properties measuring devices. In addition, the relationship between glass property models and the melter operating conditions have not advanced significantly since early studies conducted at Pacific Northwest National Laboratory (PNNL) and Savannah River Technology Center (now the Savannah River National Laboratory, SRNL) [1-7]. Current melter operations have to deal with cold cap formation and growth in order to keep up production rates. Cold cap formation also affects the melter vapor space temperature and combustion of the melter off gases, which impacts the off gas system as well as melter feed rates. Foaming of the melt also hampers melter operation, which is affected by the redox and the viscosity of the melt [8]. Excessive foaming can slow down production rate by decreasing heat transfer to the top of the melt pool and by limiting feed rates due to maximum tank levels and also potentially lead to catastrophic spills that would put personnel at risk [8, 9].

2.2. Melter Monitoring Needs

A basic melter operation problem is not being able to measure liquidus temperature on-line [9]. The liquidus temperature is important due to the formation of crystals that greatly impact the processing of the glass in the melter as well as the durability of the glass product for disposal. Another problem is accounting for the redox (ratio of reducing reactions to oxidizing reactions) of the melt pool when blending a waste batch [8-12]. A higher redox can lead to metals precipitating out and potentially shorting a joule-heated melter. If redox is too low, then foaming can become an issue since there are more oxidation reactions releasing gases. Additionally, the thermal gradients in the melt pool can impact production rates by affecting the density and viscosity of the melt, which in turn affects the ability to mix and properly pour [13]. Having the ability to measure viscosity and density of the melt pool can directly affect the production rate of a melter. To maximize waste loadings, an accurate composition of the melt pool is needed. In current melter operations, only predictions of the melt pool composition are available.

These composition predictions are used in property models to predict with the associated inherent modeling errors the glass viscosity, density, redox, and liquidus temperature. The relationship between these anomalies and the measured melter parameters is deemed to be qualitative at best [14]. This lack of on-line measuring devices/technology makes implementing a feedback control loop on glass properties impossible.

In contrast, the MMW technology could enable on-line temperature, viscosity, emissivity, and density measurement of the molten glass simultaneously. It also has the potential for measuring melter vapor space temperature and temperature of the surrounding refractory and might even be able to relate measurements back to glass composition. Glass composition is tightly related to glass properties and thus melter control [1-3, 15, 16]. Using the MMW technology as an on-line glass composition/property tool, a more robust feedback control system could be developed for a vitrification process instead of relying solely on feed-forward statistical process control predictions. In addition, the waste vitrification process has been shown to have non-linear behavior [5, 7, 17] like many processes in the chemical industry. More advanced control techniques like Internal Model Control could be adapted using the MMW on-line measurements. The ability of the MMW techniques to measure on-line glass properties could revolutionize the control of glass melters by allowing the implementation of more advanced controls.

The MMW on-line measurements could also be used to improve more than just glass property control. Being able to measure glass properties on-line versus using predictions based on time-delayed analytical data would allow smoother operation at more sustainable melter production rates. On-line monitoring could be used to mitigate problems with cold cap formation, thermal gradients, crystal formation (liquidus temperature), foaming, slow pouring rates, and metal precipitation (redox), which adversely impact melter throughput.

2.3. Cold Cap and Plenum Temperature

In most high temperature joule heated melters, a cold cap forms on top of the melt pool where the waste feed is fed and only partially vaporizes and/or melts. The vaporization and melting adsorb a great deal of melter energy and thus the top of the melter cools off. As the top of the melter cools, a crust begins to form on top of the melt pool and starts to cover the hot molten glass below. In current melter operations, there is no way to measure the extent of the cold cap coverage, which makes it difficult to control the melter temperature and processing. A cold cap also causes the melter vapor space temperature to drop due to loss of radial and convective heat from the molten glass surface. This vapor space temperature drop in turn triggers constraints on minimum temperatures for complete combustion of melter off gas which in turn shuts the feed down until the vapor space temperature goes back above the constraint. When the feed is shut off, the melter production rate drops accordingly. MMW diagnostics could be used to profile the temperature on the surface of the melt pool to monitor the status of a cold cap so control of its consistency would be possible by changing the melter blend chemicals, the melter electrode power distribution, and/or the waste feed rate.

An extension of the MMW temperature measurement capabilities would be to measure the melter vapor space temperature. Although this particular measurement technique has not been developed, it is known that MMW or submillimeter-wave radiometry could also provide this valuable measurement. The melter vapor space temperature is important to melter operation because it is the only indicator of poor combustion in the melter vapor space, which directly impacts the safety interlocks on the melter feed. If the real-time measurement capability could be extended to measuring melter vapor space temperature, a feedback control scheme could be devised to minimize impact on melter throughput. The current control scheme at DWPF uses a conservative predicted value of the melter vapor space temperature to set the feed safety interlocks.

2.4. Improving Throughput

While the vitrification processes at DWPF and those planned for WTP do function well, their ability to increase production and waste loading is limited by the bounds of the operating envelope developed by the feed forward control systems in place [19]. These feed forward control systems are based on first principle and statistical models [1-6, 11, 12, 15-17, 20-22] that are limited by errors in the property composition measurements and databases as well as the understanding of the melting process. MMW measurements would allow relaxation of some of the glass property uncertainties used to define the melter operating envelopes. In turn, it would be possible to expand the operating envelope for acceptable glass blends. The glass viscosity is a key processing constraint, since if the glass viscosity becomes too high (much greater than 100 Poise) then it will be difficult to pour the glass melt into the canisters. If the melt viscosity drops below a value of about 20 Poise, then the glass pour will be too fast and concentration gradients could occur in the glass. Melt with low viscosity is known to accelerate refractory and electrode corrosion, with other conditions that remain the same. A low viscosity may also cause problems with foaming. With an on-line glass viscosity measurement, the viscosity dynamics could be monitored real-time and the glass blending chemicals, melter power distribution, and/or feed rates could be adjusted to satisfy a measured value instead of a predicted value.

New sensor technologies like MMW techniques can be developed and applied with existing process control techniques to enhance the operation and control of currently operating and any new planned DOE vitrification facilities. Accurate non-linear modeling techniques already exist in industry [23, 24]. The data to relate melter performance to glass product quality is needed to further develop the current process control models that limit nuclear waste vitrification processes. Further expansion of these models requires developing a relationship between melter operating parameters and glass chemistry. MMW diagnostics can help bridge this gap.

3. Millimeter-Wave Monitoring Techniques

3.1. MMW Sensor Configuration

The basic configuration of a millimeter-wave sensor for multiple parameter measurements of the melt pool in a melter is shown in Figure 3 [25]. The main building blocks are the millimeter-wave heterodyne receiver, a beamsplitter in the receiver field-of-view beam, a waveguide/optics transmission line to the melt pool, a window to seal the waveguide, and a thermal return reflection (TRR) mirror aligned with the split signal from the beamsplitter. Millimeter-wave signals are both received from, and transmitted back to the molten glass. With this configuration and appropriate minor modifications, it is possible to monitor all the key melt pool parameters listed in Table 1 using only a single access point into the melter. The physical melt pool effect that is being exploited in the millimeter-wave range to obtain the measured parameter is listed in the second column. The temperature and emissivity of the monitored surface are obtained by measuring the MMW thermal radiation from the surface and using this radiation by the TRR mirror as a probe of the surface reflectivity [26]. The density and viscosity are obtained by measuring the position and flow of the surface in response to a known pressurization of the waveguide. Surface position is measured with submillimeter precision by monitoring the phase of the surface refection of a leaked nonthermal oscillator signal from the receiver. Foaming, salt layer, and other melt pool properties are obtained by combinations of the thermal and nonthermal emission and reflection measurements.

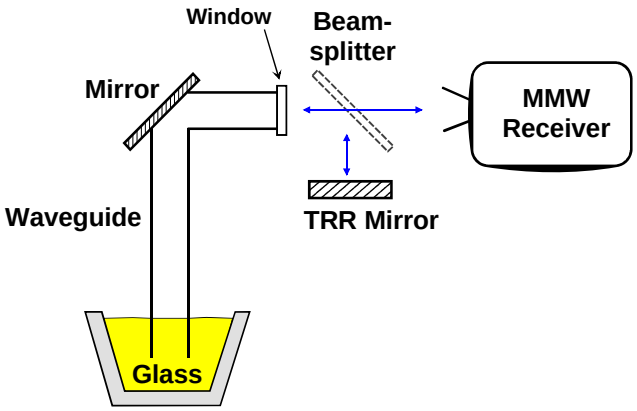

Figure 3. Basic millimeter-wave sensor configuration.

Table 1. MMW Measurements

Melt Parameter	Measured MMW Effect
Temperature (T)	Thermal emission
Emissivity (ε)	Reflection amplitude
Density (ρ)	Reflection phase
Viscosity (η)	Reflection phase rate
Foaming	Surface acceleration/emissivity
Salt Layer	Emissivity/turbulence

Achieving the sensor configuration as shown in Figure 3 required developing novel millimeter wave components suitable for use in the high temperature and industrial environment of a nuclear waste glass melter. These components are the high temperature waveguide that interfaces with the hot melt pool and the quasi-optical beamsplitter TRR mirror configuration that is both rugged and efficient in the MMW wavelength range. These component developments along with the heterodyne receiver are summarized below after the analytical basis is established for the MMW measurements. Following this section the laboratory/field measurements that have been made to test the performance to this technology are summarized. It should be noted that Table 1 is not comprehensive. It shows only the parameter measurements that have been demonstrated so far by the MMW technology. Additional melt pool parameter measurement capability

for liquidus temperature, redox potential, noble metals precipitation, plenum temperature, and others are potentially possible with future development.

3.2. Analytic Basis for Temperature and Emissivity

Thermal emission signals are proportional to the product of the emissivity and temperature (εT) of the material that is viewed, where emissivity (ε) is a factor between 0 and 1 specifying how close the viewed material is to a perfect black body. All current pyrometers require some assumption on emissivity in order to determine temperature. Methods that can resolve the emissivity and temperature in real-time would be of great value to thermal analysis because they would not only improve temperature measurement accuracy, but would also provide information of the properties of the viewed material. The TRR method described here makes it possible to resolve of the temperature and emissivity parts of the thermal emission from a surface that is oriented normal to the viewing direction and is relatively smooth to the viewing wavelength (a distinct advantage for the longer MMW wavelengths over infrared pyrometry). The basic concept is to use the thermal radiation from the viewed source as a probe of its emissivity. Earlier work using a coherent oscillator signal to probe surface reflectivity required taking into account coherent standing wave interference [27]. The use of incoherent thermal radiation as the probe beam eliminates coherent interference and greatly simplifies and improves the reliability of the reflection measurement to determine emissivity.

The analytical basis of the TRR method to monitor temperature and emissivity requires taking into account all sources and losses of the thermal radiation between the source and receiver as viewed by the receiver. The main components of the MMW sensor are shown in Figure 4 along with the thermal parameters that enter into the analysis. The receiver views a sample (S) through a beamsplitter (BS) and waveguide system (WG). Each component has associated with it an emissivity (ε), temperature (T), transmission factor (τ), and/or reflectivity (r). If a component is at room temperature, then its emissivity and temperature will not contribute to the final result since the receiver is calibrated against room temperature. For example, the beamsplitter is at room temperature and its emissivity does not contribute. On the other hand, the waveguide, which is partially inserted into the melter and is on average higher than room temperature, must have its contribution to the thermal signal as seen by the receiver taken into account.

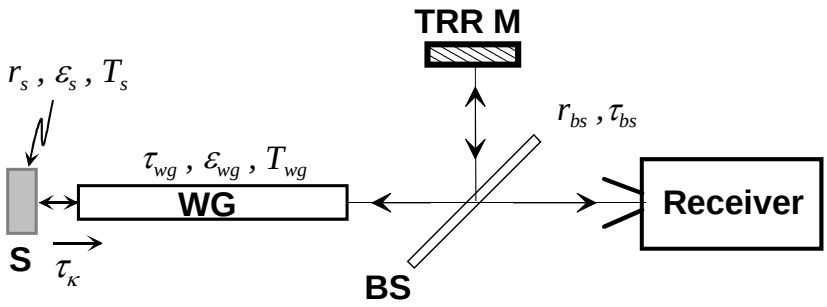

Figure 4. Illustration for defining the terms used in deriving the analytical basis for the TRR method.

Two temperature signal measurements are made with the MMW sensor system. One with the TRR mirror blocked and a second with the TRR mirror unblocked sending a portion of the thermal emission back as a probe of the viewed sample reflectivity. The sample is assumed to be completely opaque with no transmission through it. The analytical results for the measured temperature at the receiver for these two TRR cases are given by [28]:

$$T_{eff} = \varepsilon_{wg} T_{wg} + \tau_{wg} \varepsilon_s T_s + r_s \tau_\kappa \tau_{wg} \varepsilon_{wg} T_{wg} \tag{1}$$

$$T_{eff}^{'} = \frac{T_{eff}}{1 - r_s \tau_\kappa r_{bs}^2 \tau_{wg}^2} \tag{2}$$

where T_{eff} and $T_{eff}^{'}$ are the effective MMW temperatures measured at the receiver without and with the TRR, respectively, T_{wg} and T_s are the waveguide and melt surface temperatures, ε_{wg} and τ_{wg} are the waveguide emissivity and transmission related by $\varepsilon_{wg} = (1 - \tau_{wg})$, ε_s and r_s are the emissivity and reflectivity of the viewed surface related by $\varepsilon_s = (1 - r_s)$, r_{bs} is the beamsplitter reflectivity, and τ_κ is the viewed surface coupling factor. These two equations can be solved to obtain the emissivity and temperature of the viewed sample. The explicit expression for the sample emissivity is given by:

$$\varepsilon_s = 1 - \frac{1}{\tau_k r_{bs}^2 \tau_{wg}^2} \left(1 - \frac{T_{eff}}{T_{eff}^{'}} \right) \tag{3}$$

where the ratio of the two effective MMW temperatures are obtained from the measurements, r_{bs} and τ_{wg} are previously determined instrumentation parameters, and τ_κ can be assumed to be equal to one if the waveguide is very close to the surface (less than the inner radius of the waveguide) and the surface is aligned to perfectly reflect a MMW signal back to the receiver. The result of Equation 3 can then be used with Equation 1 to obtain the sample temperature. If surface roughness is large relative to the wavelength or alignment is not perfect then τ_κ can not be assumed to be one and other means would

need to be used to estimate this factor. Assuming it to be equal to one would in this case only give an upper limit to the actual emissivity.

3.3. Viscosity

Viscosity is related to melt glass flow, which is measured by the sensor configuration as shown in Figure 3 by immersing the waveguide into the molten glass and pressurizing the waveguide to displace the glass. In practice, the waveguide is pressurized first to displace the glass melt inside the waveguide and then suddenly the pressure is released by an electrically operated solenoid valve. The rate of flow of the glass melt back into the waveguide under the force of gravity to refill the waveguide is then measured and related to viscosity. This is analogous to the standard room temperature laboratory capillary flow technique for viscosity measurement, but implemented at high temperatures using the refractory waveguide as the "capillary" and the millimeter wave receiver instead of a stopwatch to determine rate of flow.

The actual molten glass surface displacement is determined by monitoring the reflection of the leaked local oscillator (LO) from the MMW receiver. The phase of the coherent LO reflection depends on the path length between the receiver and melt surface. For a path length change of one half wavelength, the phase will change by π or 180°. If the signal is initially in phase (maximum signal), then it would go completely out of phase (minimum or zero signal) for every half wavelength change in path length. Figure 5 illustrates how this signal will appear for an example displacement shown by the top curve and an LO frequency of 137 GHz (λ = 2.2 mm). For every quarter wavelength (¼λ) displacement of the melt level (round trip MMW path length change of ½λ), the video signal will cycle through a minimum–maximum period (fringe) corresponding to a round trip reflection phase shift of π. This is similar to a Michelson interferometer [29] in which the moving mirror against a fixed mirror generates fringe patterns. For a linear displacement the video signal will appear as a rectified cosine function as shown in the

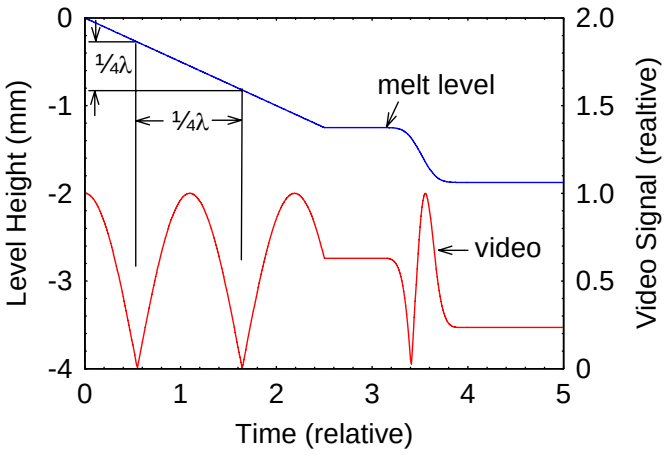

Figure 5. Calculated illustration of the relationship between melt level height change and a millimeter-wave video reflection signal at a frequency of 137 GHz (λ = 2.2 mm).

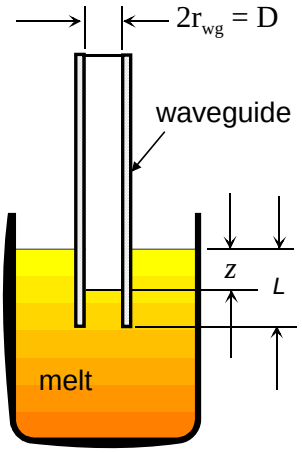

Figure 6. Definition of terms used for derivation of analytic basis of viscosity.

beginning of the lower plot in Figure 5. For a non-linear level change, the video signal fluctuations will be distorted from a cosine function as shown in the latter part of the plot in Figure 5. In the case of molten glass refilling the waveguide, the flow observed is typically a gradually slowing rate. Counting the number of fringes and multiplying by ¼λ will give the total distance the melt surface has moved and dividing by the time period of the movement will give the average velocity of the flow.

A simplified Navier-Stokes [30] analysis for laminar flow of a Newtonian fluid in a pipe can be used to derive a relationship between the observed measured average waveguide refilling velocity and the molten glass viscosity. With the definition of terms as shown in Figure 6 this equation is given as:

$$v_{ave} = A\rho \frac{z_o}{(L - z_o)\eta} \tag{4}$$

where A is an instrumentation constant, ρ is the molten glass density, z_o is the initial glass displacement, L is the waveguide immersion depth, and η is the glass dynamic viscosity. The instrumentation constant can be determined by making a measurement of a melt with a previously determined viscosity. The melt density can in principle be obtained from the measured fluid displacement for the known waveguide pressurization.

An even simpler form of Equation 4 is possible if the initial glass displacement and waveguide immersion are kept constant for all measurements. In this case the relation between flow rate and viscosity in the waveguide is analogous to the Ubbelohde or Cannon Fenske type capillary viscometers where the relationship between kinematic viscosity and the time for flow, Δt, between two fixed positions in the waveguide is given by [31]:

$$\nu = C\Delta t \tag{4a}$$

where C is a constant that incorporates the instrumentation constant A as well as the waveguide immersion dept and pressure displacement. The dynamic viscosity is related to the kinematic viscosity as $\eta = \nu\rho$. The millimeter-wave viscometer measurement is therefore directly analogous to the conventional capillary flow viscometer method where the capillary in this case is the MMW waveguide.

4. Millimeter-Wave Monitoring Technologies

4.1. MMW Receiver

The heart of the MMW sensor configuration for melter monitoring is a MMW receiver system that has the sensitivity to detect the thermal emission from the melter and at the same time leak an oscillator signal for position measurements. It is based on a heterodyne receiver, the main elements of which are shown in Figure 7. A MMW mixer is used with a local oscillator (LO) to down convert the MMW thermal signal to an intermediate frequency (IF) in the microwave frequency range for amplification and detection. A heterodyne receiver naturally leaks a part of its LO out the horn antenna, which is used for melt surface position measurements. A chopper modulates both the thermal signal and the leaked LO to make possible the detection of very weak signals with lock-in amplifiers that are only sensitive to the chopper frequency. A bias tee at the mixer output separates the IF thermal signal from the low chopper frequency position signal (video) to separate channels for amplification and detection.

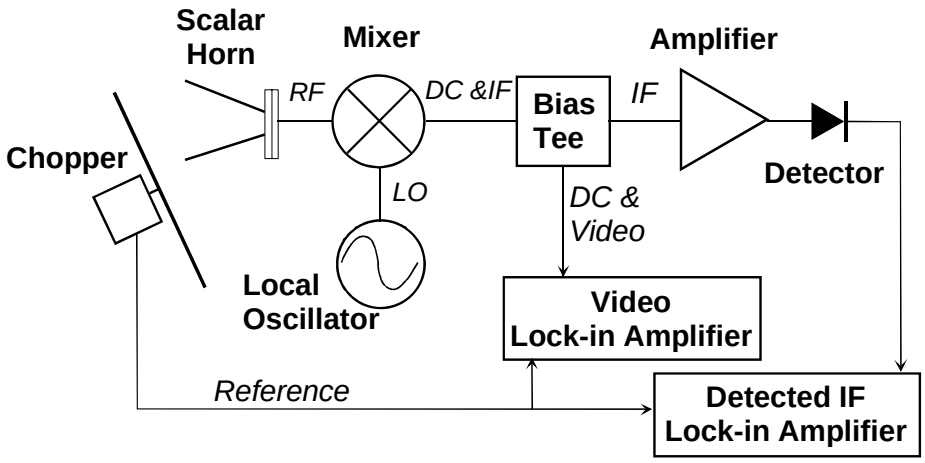

Figure 7. Millimeter-wave heterodyne receiver system for thermal emission and surface position measurements.

The chopper also functions as a room temperature reference source for the thermal measurements in the manner as originally described by Dicke [32]. When the chopper bladed blocks the receiver field-of-view the receiver sees room temperature emission off the blade. When the receiver field-of-view is not blocked by the chopper blade the receiver sees the thermal emission from the melt surface. The IF lock-in amplifier detects this difference signal. A thermal difference signal can be produced by viewing either a hot or cold source relative to room temperature, making it convenient to calibrate the receiver with a cryogenic source such as one cooled by readily available boiling liquid nitrogen at a temperature of -196 C. The expression for the receiver measured effective temperature at the position in the view beam where the calibration source is inserted is given by:

$$T_{eff} = \frac{V_s}{V_c}\left(\left|T_c\right| - T_r\right) + T_r \qquad (5)$$

where V_s is the detected IF signal when viewing the melt surface, V_c is the IF detected signal when viewing the calibration source at temperature T_c, and T_r is the room

temperature. Consequently, the accuracy of the thermal emission measurement is determined by how well the calibration signal and room temperature are known.

Another important point is that the internal noise temperature of the receiver needs to be several times higher than the maximum melter temperature being monitored to insure a linear relationship between the measured signal and temperature. The typical microwave detector diode is not a linear detector. By keeping the internal noise signal on the detector diode large relative to the desired signal, the diode is kept at approximately a constant voltage on its response curve. For example the receiver noise temperature in the measurements presented below was typically in the range of 10,000 to 15,000 K for maximum melter measurements of up to 1,600 °C. A high receiver noise temperature does not mean that it will have poor measurement precision. Wide bandwidth and long signal integration times compensate for high noise temperature. The expression for minimum resolved temperature is given by [33]:

$$\Delta T_{\min} = \frac{T_i}{\sqrt{tdf}} \tag{6}$$

where T_i is the receiver noise temperature, t is the signal integration time, and df is the receiver double sideband (DSB) bandwidth. For a receiver with a noise temperature of 15,000 K and a DBS bandwidth of 3 GHz, typical for some of the measurements presented below, the temperature resolution is 0.3 °C for one second integration times. Such temperature precision and time resolution is more than adequate for most melter measurements.

4.2. High Temperature Waveguides

Interfacing the MMW receiver system with the melter requires an efficient millimeter-wave waveguide that can survive temperatures over 1000°C inside the melter and immersion into the melt pool itself for viscosity measurements. Luckily, efficient hollow millimeter-wave waveguides can be fabricated from almost any refractory material such as those used to fabricate melter crucibles. This is accomplished by making the waveguide diameter much larger that the wavelength and using the HE_{11} waveguide mode (transverse magnetic and electric fields) for propagation [34]. The HE_{11} mode is a natural mode inside smooth walled dielectric tubes (the same mode is used inside single mode fiber optic cables at light wavelengths) and can be propagated inside electrically conducting metallic tubes by circumferentially corrugating the inside wall with ¼ λ deep grooves at more than 2.5 grooves per λ of waveguide length [34]. The HE_{11} mode is also ideally suited for monitoring applications because it launches as a free space Gaussian beam, which is optimum for achieving the smallest possible diffraction limited spot sizes for good spatial resolution.

The power transmission factor for a waveguide is given by the exponential relation:

$$\tau_{wg} = e^{-2\alpha z} \tag{7}$$

where α is the waveguide electromagnetic field attenuation coefficient and z is the waveguide length. The electromagnetic field attenuation coefficient has been derived for HE_{11} mode propagation for both the circular smooth walled dielectric and corrugated walled metallic waveguide types. For a hollow circular dielectric waveguide with thick waveguide walls that are opaque to millimeter-wave leakage through the side it is given as [35]:

$$\alpha = 0.0733 \frac{\lambda^2}{a^3} \frac{\left(n^2 + 1\right)}{\sqrt{\left(n^2 - 1\right)}} \tag{8}$$

where a is the waveguide internal diameter and n is the index of refraction of the dielectric waveguide walls. For circular corrugated metallic wall waveguide with large inside diameter > 3λ it is given as [34]:

$$\alpha = 1.94 \times 10^{-4} \frac{\lambda^2}{a^3} R_s \tag{9}$$

where R_s is the metal wall surface resistivity in ohms. The surface resistivity is given by $R_s = \sqrt{\pi f \mu_o / \sigma}$ where f is the frequency, μ_o is the permeability constant (1.26×10^{-6} henry/m), and σ is the metal conductivity.

It can be seen from Equations 8 and 9 that the transmission losses through the waveguide are proportional to λ^2/a^3. Consequently, they can be made as small as necessary by making a sufficiently large relative to the wavelength. Also, the smooth walled dielectric waveguide needs to be about 10 times larger in diameter than a corrugated metallic waveguide to achieve the same losses. A poor metallic conductor (by microwave standards) with a high surface resistivity can also be used to make an efficient waveguide as was shown with a circular corrugated graphite waveguide used in a non oxidizing furnace [36].

A MMW waveguide configuration developed for use in the oxidizing environment of nuclear waste melters and used for many of the measurements presented below is shown in Figure 8. It consists of a room temperature corrugated brass waveguide section connected by a flat 90° turning miter mirror to a ceramic waveguide section to access the high temperature environment of a melter from the top. Both sections have an internal diameter of 28.6 mm (1 1/8 inch). The MMW receiver frequency used in the tests was 137 GHz (λ*=2.19 mm*) and the corrugation dimensions shown for the brass section are optimum for this frequency. According to Equations 7 and 9 the transmission efficiency of the brass waveguide (R_s *= 0.2 ohm at 137 GHz*) is about 10^{-4} dB/m or about a 1% loss for 650 m length. Therefore, this waveguide section could be made as long as necessary to transmit the millimeter-wave signal outside the biological shield of a nuclear waste glass melter facility.

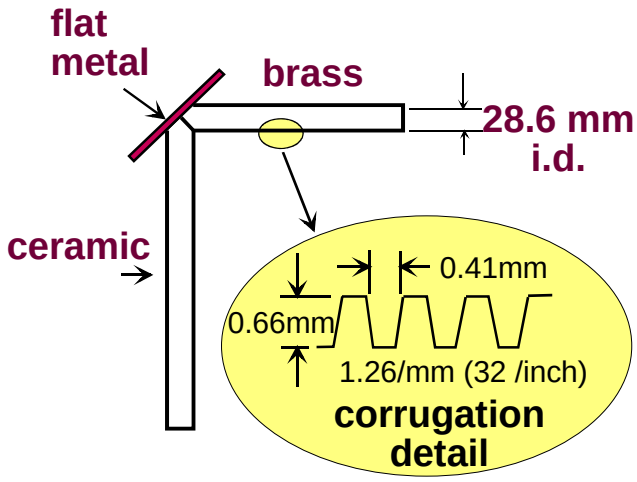

Figure 8. MMW waveguide used for many measurements was a composite of room temperature corrugated brass and high temperature ceramic sections. The corrugation dimensions are shown for a frequency of 137 GHz.

The ceramic waveguide waveguide section used for most measurements was a mullite ($3Al_2O_3 \cdot 2SiO_2$) tube. Mullite was chosen because it was relatively robust to glass melt immersion and has somewhat higher losses for MMW transmission through the sidewalls than the pure alumina or silica materials. Even so, the commercially available wall thickness of 3.2 mm (1/8 inch) was not sufficient to satisfy the condition of Equation 8 for completely MMW opaque side walls. The predicted transmission factor of τ_{wg}= 0.7 for a 50 cm long 28.6 mm diameter mullite tube at 137 GHz ($n \approx 2.5$), in practice, varied over the range 0.6 to 0.8 from tube to tube due to poor tolerance on wall thickness. The higher transmission loss of the ceramic waveguide section necessitated keeping this section as short as possible, typically ≤ 50 cm, only long enough to access the high temperature environment. For some of the laboratory studies a larger diameter brass-mullite waveguide assembly of 41 mm (1 5/8 inch) diameter was used which had a transmission factor of about 0.9 for the 50 cm long mullite section.

Tests were carried out at temperatures of up to 1500°C and with waveguide glass immersions for up to one week in nuclear waste glass melts. Good MMW performance results were achieved. Some penciling (corrosion) of the immersed mullite waveguide was observed, but did not affect the millimeter-wave performance significantly in the tests to date. Advanced refractories could be used to make the waveguide last as long as the melter crucible. This waveguide technology also has important spin off applications to monitoring in nuclear fusion experiments, nuclear power plants, fossil fuel power plants, and manufacturing where diagnostic access to high temperature environments is extremely challenging [37, 38].

4. 3. Compact Quasi-Optical Beamsplitter/TRR Mirror

In addition to the waveguide a MMW signal control component is required to implement the temperature and emissivity monitoring function. At high MMW frequencies optics are the most efficient way of achieving beam splitting and redirection of signal, but MMW optics are large and very sensitive to alignment. In an industrial scale nuclear waste melter environment, it is not desirable to have sensitive optics that take up a lot of space. Therefore, a quasi-optical corrugated waveguide and beamsplitter device have been developed that achieves the TRR function shown in Figure 3 in a compact, rugged component. A cross-section of this device is shown in Figure 9.

Crossed corrugated waveguides are machined in an aluminum block with a diagonal spilt as shown to accept a beam splitter. In the experiments carried out so far at 137 GHz, the waveguide block was only 6.4 cm (2.5 inches) square by 3.8 cm (1.5 inches) deep with a quartz beamsplitter. The MMW signal from the melt and receiver field-of-view transverses the block in one direction and the split signal is directed in an orthogonal direction to a TRR mirror (not shown). Insertion losses were measured to be only 0.5%. This component has been very successful in the Environmental Management Science Program (EMSP) sponsored work and has been copied by an National Institute of Health (NIH) sponsored experiment to monitor a 250 GHz gyrotron beam for dynamic nuclear polarization (DNP) measurements [38]. At frequencies above 100 GHz, this is the most efficient approach to compactly monitor MMW beams.

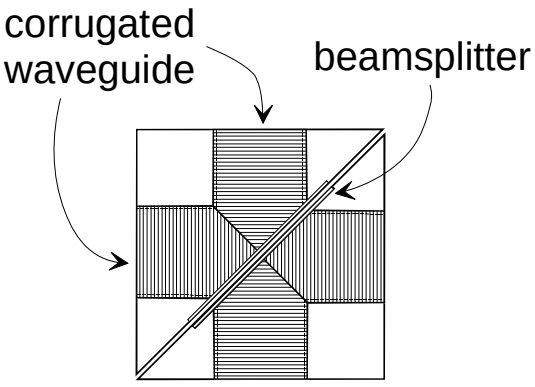

Figure 9. Quasi-optical beamsplitter. corrugated waveguide block.

5. Laboratory Measurements

5.1. Temperature and Emissivity Measurements of Advanced Refractories

The performance of the MMW instrumentation for monitoring temperature and emissivity is illustrated by a laboratory study at 137 GHz of two advanced refractory materials, alumina-zirconia-silica (AZS) and Monofax K3. Horizontally level and flat samples of these refractories were put inside an electric furnace (Deltech model DT-31-RS-12) less than 7 mm from the aperture of the mullite waveguide inserted vertically through the top of the furnace. Measurements were carried out to temperatures of up to 1500°C.

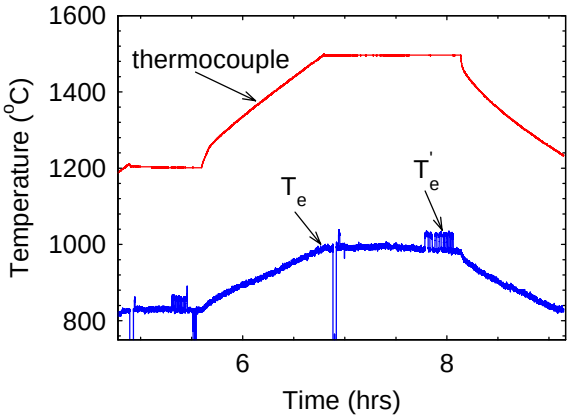

Figure 10. MMW measurements of Monofax K3 refractory.

The data for Monofax K3 is shown in Figure 10 where the top trace is the furnace temperature measured by a type S thermocouple and the bottom trace is the MMW thermal emission signal as calibrated just outside the Teflon waveguide window. The effective MMW temperature at the waveguide window is lower than the thermocouple temperature because the emissivity and waveguide transmission losses are not taken into account in this plot. The 3 mm (1/8 inch) thick Teflon window used for these measurements had moth eye

antireflection surfaces [39] and was measured to have less than 2% losses. Over a period of several hours, the Monofax K3 was first heated to 1200°C and then to 1500°C for TRR measurements as indicated by the raised structures on the plot during flat operation at these two temperatures. An expanded view of the TRR measurement at a furnace temperature of 1500°C is shown in Figure 11. The upper temperature is measured with the TRR mirror unblocked; sending a part of the thermal emission back to the refractory for an additional reflection from the viewed surface, and the lower temperature is with the TRR mirror blocked for a completely passive thermal signal measurement. Using the ratio of these two temperatures in Equation 3 the emissivity was found to be about 0.70 at both temperatures showing that Monofax K3 is a relatively stable MMW material at high temperatures.

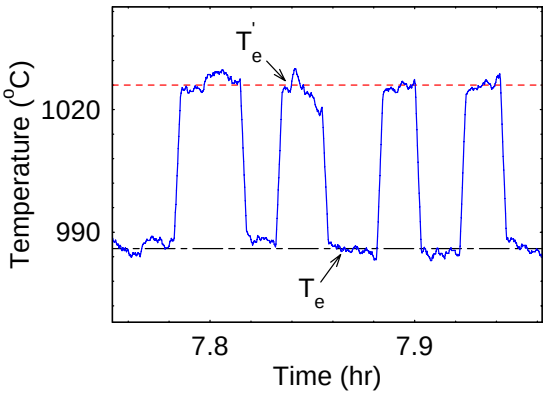

Figure 11. Expanded view of TRR measurement at 1500° C shown in Fig. 10.

Similar measurements of AZS, shown in Figure 12, revealed it to be unstable at the highest temperatures studied. Again, the top trace shows the furnace thermocouple temperature and the bottom trace the millimeter-wave temperature as calibrated at the waveguide window. The AZS was heated to five temperature steps between 1000 and 1500°C. At each step a TRR measurement was made as shown on the millimeter-wave signal by the upward structures. At the temperature transition from 1400 to 1500°C the millimeter-wave signal makes a sudden increase greater than that expected by the thermocouple reading, indicating that the emissivity of the AZS increased anomalously. The TRR data shows that the emissivity gradually decreases from about 0.70 to 0.60 over the temperature range of 1000 to 1400°C and then makes an abrupt increase to about 0.76 in the flat top region at 1500°C, a 25% jump in emissivity. Examination of the AZS sample after the furnace cooled down showed that a glass phase from inside the sample had eluded out, changing the surface chemistry and figure. Consequently, the AZS would be unacceptable to use as a MMW waveguide component at high temperatures. Measurements of other refractory materials [31] in addition to

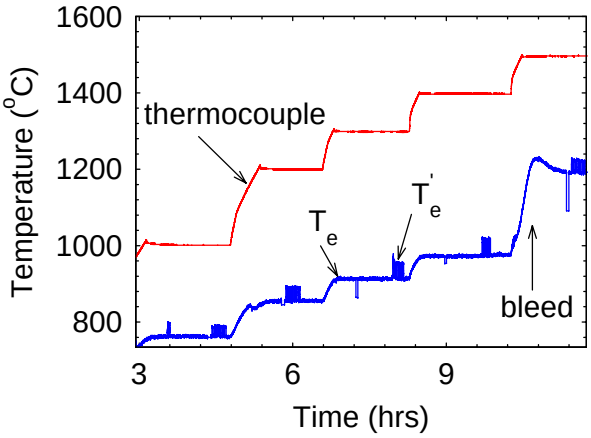

Figure 12. MMW measurements of alumina-zirconia-silica (AZS) slowing glass bleeding above 1400°C

Monofax K3 did not reveal unstable MMW behavior. These measurements illustrate the usefulness of millimeter-wave TRR for high temperature thermal analysis of materials [40].

5.2. Viscosity

Millimeter-wave laboratory glass flow data as a function of temperature was taken for a number of glass compositions that included two Hanford glass mixes, DWPF black frit #265, and a commercial E glass. The connection of molten glass flow time in the waveguide with viscosity was empirically established. It was also found that surface tension effects appear to dominate at the end of the flow time when the surface is relaxing to equilibrium and when the displacements are small in the waveguide. The fact that surface tension plays a role in the waveguide melt flow was also seen in the overall reflected signal amplitude variation with changes in pressurization, which effected surface curvature and refection coupling (τ_k) to the waveguide HE_{11} mode. Consequently, the difference in flow time between two pressure displacements was used to subtract out the common starting and ending surface curvature motions to achieve a reliable viscosity measurement minus the surface tension effects. The resulting time difference with this subtraction corresponds only to the laminar flow time in the waveguide.

Representative reflection signals for two pressurizations of Hanford #8 glass (target composition 56.8% SiO_2, 20% Na_2O, 12% Al_2O_3, 9% B_2O_3, and several other trace oxides) at a temperature of 1000°C in 28.6 mm diameter mullite waveguide are shown in Figure 13. The waveguide was immersed about 25 mm into the melt in a 76 mm diameter crucible with at least 50 mm of depth of glass in a Deltech model DT-31-RS-12 furnace. In the top Figure 13a, the waveguide was pressurized with nitrogen to 0.48 inch (12 mm) water pressure above atmosphere and in the lower Figure 13b, the pressurization was to 1.2 inch (30 mm) water. After pressurization and allowing 2 to 3 minutes for the glass melt to reach equilibrium at the higher pressure, a computer controlled valve was opened at time zero as shown on the plots to release the waveguide pressure back to atmosphere. The flow of the melt back into the waveguide pipe is recorded by the fringes in the plots, one fringe corresponding to a displacement of approximately 0.55 mm. Alternate fringes appear strong and weak because of a

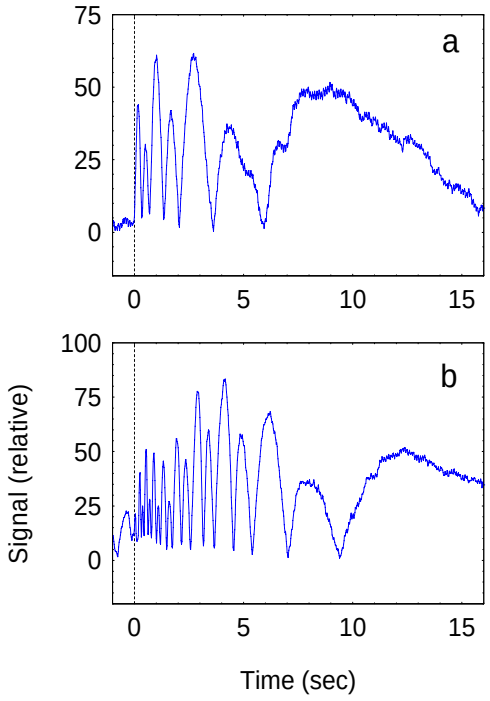

Figure 13. Hanford #8 glass flow signal in 28.6 mm diameter waveguide at 1000°C after pressurization to a) 0.48 inch (12 mm) and b) 1.2 inch (30 mm). Each fringe corresponds to 0.55 mm displacement.

signal offset in the lock-in amplifier. The envelope of the fringe pattern varies from a low to high and back to a low level as the surface curvature flexes in response to the sudden flow, changing the focusing of the reflected signal back into the waveguide. Counting the fringes, there are seven for the 12 mm pressurization and eighteen for the 30 mm pressurization corresponding to melt displacements of 3.9 and 9.9 mm, respectively. The ratio of these measured displacements to the pressurization results in a factor of about 3.0, which is not an accurate determination of the specific gravity for this melt. Room temperature measurement of this glass showed that the specific gravity is about 2.5. Even if the finite dimensions of the crucible are taken into account, it is evident that there is additional resistance to the flow in the waveguide. However, this additional resistance factor appears to be a constant over a wide range of melt viscosity.

The measured waveguide flow time for the Hanford #8 glass between 0.5 inch and 1.2 inch pressure displacement is plotted in Figure 14 as open squares against viscosity as determined by Corning Services Laboratory for this glass. Varying the temperature of the glass from 850 to 1200 °C varied the viscosity over the range of 2000 to 20 Poise. The data is plotted on a log-log plot because of the wide dynamic range of the measurements. The line through the experimental points is a linear fit to the experimental points corresponding to Equation 4a with the constant density product given by $C\rho$ = 58 Poise/sec. The measured flow time tracks the viscosity perfectly over a 100:1 dynamic range of 20 - 2000 Poise. Accurate viscosity measurement over such a large dynamic range is a unique capability of MMW viscometer in addition to the high temperature operation. These laboratory viscosity measurements not only established the viability of MMW viscosity measurements, but also revealed interesting surface dynamics that would be of interest for future study [40]. One of these interesting observations is submillimeter surface turbulence that increases inside the trapped volume of the sealed waveguide versus an unsealed waveguide.

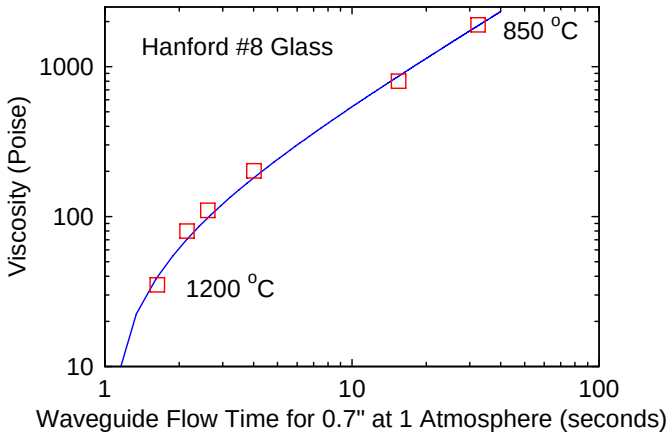

Figure 14. Glass viscosity versus the flow time in a millimeter-wave waveguide.

5.3. Foaming

A combination of the MMW monitoring capability for temperature, emissivity, and surface motion can be used to detect a glass melter foaming event. Vitrification operations at DWPF have encountered sudden glass foaming events that seriously disrupt the operations. On-line monitoring that can alert operators to the onset of foaming would be of great value. MMW laboratory measurements with hi-foaming glass have shown

that MMW measurements can not only monitor a foaming event, but also can provide a precursor indication long before the foaming gases break the melt pool surface [41].

The data for a 3-inch (76 mm) diameter crucible melt which was formulated to foam (target composition 45.3% SiO_2, 15.3% Na_2O, 8% Al_2O_3, 7% B_2O_3, 0.3% Cr_2O_3, 11.5% Fe_2O_3, 4.5% Li_2O, 6% ZrO_2, and several other trace oxides) is shown in Figure 15. The top trace shows the furnace thermocouple signal, the next trace below shows the MMW thermal signal (εT), and the bottom trace is the surface position video signal. The events of the foaming unfold as follows: 1) at about 65 minutes on the x-axis the surface begins to accelerate as evident by the rapid fringe shifts on the video signal, 2) shortly after the onset of surface acceleration, the MMW thermal signal begins to approach the thermocouple temperature signal (emissivity increasing), it peaks at about 80 minutes on the x-axis, 3) after peaking, the MMW thermal emission decreases, gradually at first and then abruptly at about 100 minutes on the x-axis. When the MMW thermal signal increases, the video reflection signal from the melt surface decreases. At the peak MMW emission, the video signal is approximately zero as would be expected for a surface that has gone to an emissivity of one ($\varepsilon = 1$). At this point, the MMW radiation temperature equals the thermocouple temperature, if the waveguide losses are taken into account. The MMW temperature plot in Figure 15 has been normalized to the thermocouple temperature at this point.

A possible interpretation of these measurements is as follows: 1) dissolved gases come out of the melt pool solution and begin pushing on the surface displacing it in the MMW view, 2) it takes about 15 minutes for the gases to reach the melt surface in the 3-inch crucible before they begin to effect the surface emissivity, 3) when the bubbles break the surface, they initially cause a roughening of the surface on MMW scale lengths to prevent reflections and then gradually coalesce to reform a uniform surface, eventually forming a large bubble that pops. If this interpretation is accurate, it will be of great usefulness for nuclear waste glass monitoring. On the much larger scale dimensions of nuclear waste glass melters, it is likely that it would take more time to build up gases below the melt surface before significant foaming occurs on the surface. Monitoring for the onset the MMW surface acceleration and change in surfaces emissivity could therefore give nuclear glass melter operators a longer time than these laboratory measurements before the advent of significant

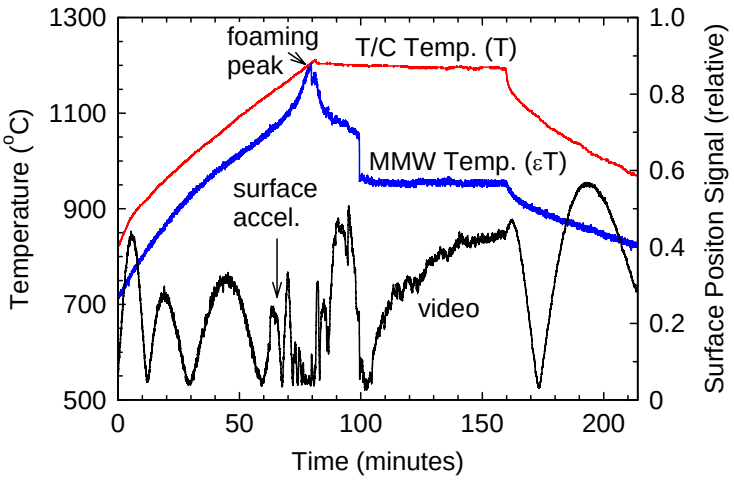

Figure 15. MMW signal record of hi-foaming glass as it is melted down.

foaming gas releases. Corrective action could then be taken to mitigate the onset of foaming. However, the results in Figure 15 are only preliminary and more research is need to establish this monitoring technique for foaming and to exploit this technique for a better understanding of the physics and chemistry of a melter foaming event.

6. Melter Tests

Tests of the MMW monitoring technology have been carried out on engineering pilot scale glass melters. Melter tests achieve two goals: 1) they demonstrate to the melter community that millimeter-wave monitoring technology is not a laboratory curiosity but fully capable of functioning reliably in a 24/7 manufacturing environment and 2) they provide access for research with full scale melt pools having continuous top feeding with a cold cap, deep melts with temperature gradients, and glass pour events that cannot be easily simulated in the laboratory. Field tests were carried out on the EnVitco (EV-16) joule heated melter at the Clemson Environmental Engineering Technology Laboratory (CETL) and at the Slurry Fed Melt Rate Furnace (SMRF) at Aiken County Technology Lab (ACTL) at the Savannah River National Laboratory (SRNL). The EV-16 melter has a melt pool size of 18″x 18″x 14″ (46 cm x 46 cm x 36 cm) and is powered typically at 70 kW in two zones by four molybdenum electrodes, one centered in each wall below the melt surface. The SMRF is a smaller melter having dimensions of 8″ x 8″ x 8″ (20 cm x 20 cm x 20 cm) with one heating zone.

6.1. Cold Cap Measurements

The goal of the first test on EV-16 was to demonstrate two dimensional MMW temperature measurements of the melt surface with and without a cold cap. The cold cap is a solid crust in top fed joule heated melters, playing a key role in feeding, stabilizing the vitrification process, and maintaining glass production rates. On-line monitoring of the cold cap would improve process control, increase production, and reduce costs for waste vitrification. For these measurements, the MMW waveguide was modified as shown in Figure 16. An Inconel miter mirror cap was attached to the end of a mullite waveguide, which was inserted horizontally into the melter plenum area above the melt pool. The waveguide could be rotated and retracted in and out manually to scan the millimeter-wave receiver field-of-view across the surface of the melt pool.

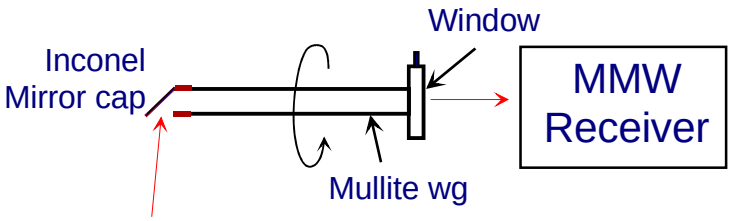

Figure 16. Rotating waveguide that was horizontally inserted into the plenum area above the melt pool in the EV-16 melter.

The MMW receiver could clearly identify hot and cold regions of the cold cap or melt surfaces and their dynamics during processing. Figure 17 shows a photo of the melter cold cap with the movable MMW waveguide entering from the right and an overlay of a surface temperature scan that was taken with the waveguide. The front center of the cold

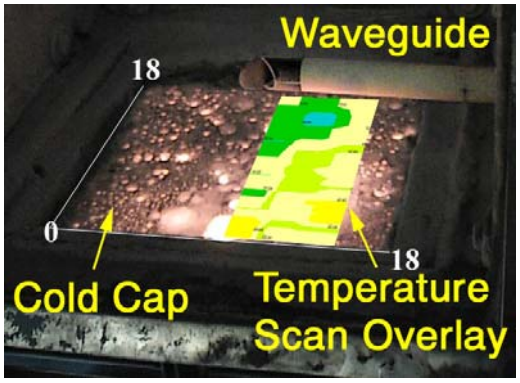

Figure17. EV-16 melter cold cap and MMW scanned surface temperature. Hotter regions are lighter and yellow in color, and colder regions are darker and green and blue.

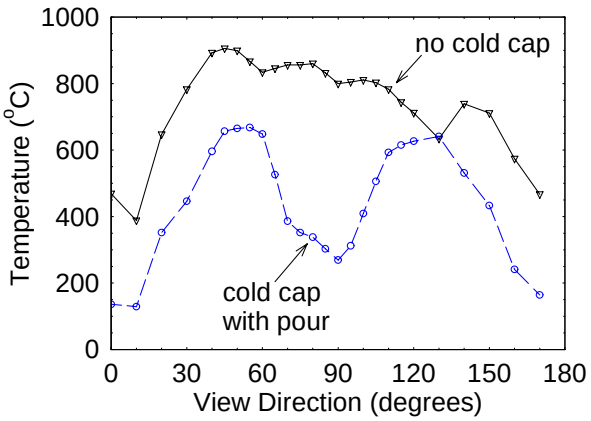

Figure 18. Melt pool surface temperature profiles.

cap above one of the electrodes is identified as being hotter than the back of the cold cap where there are no electrodes. The temperature varies form a high of about 930°C in the front hot spot to a low of about 680°C in the back cold spot. In Figure 18 two temperature surface profiles crossing near the center of the melter are shown. The scans are from front to back across the melter surface. The top trace is with no cold cap and shows a surface temperature gradient that is indicative of how the power was distributed among the electrodes below. The lower trace shows the cold cap temperature profile during glass pour from a spout below the center of the melter. There is a clear drop in surface temperature by more than a factor of two above the location of the pour spout. These measurements demonstrated, for the first time, that on-line monitoring of melter melt pool surface dynamics are possible and that the millimeter-wave instrumentation works reliably in a glass manufacturing scale melter [42].

6.2. Viscosity

In the second test at EV-16, the goals were to demonstrate the feasibility of monitoring viscosity and salt layer formation in an engineering scale melter. For these tests, the MMW waveguide was configured as originally shown in Figures 3 and 8 so that the mullite waveguide could be vertically lowered into the melt pool. Glass flow was measured over a 1″ to 8″ (25 to 203 mm) waveguide immersion range for a series of pressurizations from 0.5″ water (0.9 mm Hg) to a maximum of 12″ water (22.4 mm Hg) pressure at the deepest immersion. The average waveguide refilling glass flow velocity measured for two of the initial waveguide pressurizations of 2″ (2.8 mm Hg) and 4″ (5.6 mm Hg) are plotted as inverted triangles and squares, respectively in Figure 19. Also plotted is a temperature profile measured with a thermocouple. Equation 4 is plotted as the two dashed curves assuming viscosity is inversely proportional to temperature

($\eta \propto 1/T$). Both calculated plots were fit to the same point at 2″ (2.8 mm Hg) pressurization at a depth of 2″ (5 cm) to obtain the instrumentation constant. The general trends of the measured flow velocities with depth and pressurization are reproduced reasonably well by the assumed model. The discrepancies can be explained by effects not modeled such as temperature gradients, drifts in temperature during the course of the measurements, and deviations from the laminar flow assumption, particularly at the shallow depths when immersion depth and displacement are similar. These results demonstrated, for the first time in a glass melter, a capability for not only on-line viscosity monitoring, but also for obtaining viscosity profiles within the melt [43].

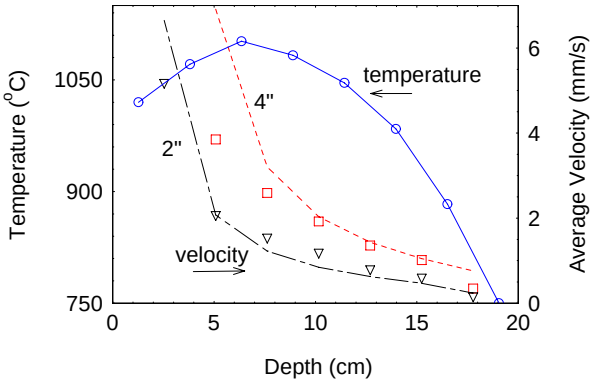

Figure 19. Temperature and melt flow velocity measurements and comparison with simple viscosity theory (dashed curves).

6.3. Salt Layer Formation

Formation of salt pools in nuclear waste glass joule-heated melters is of considerable concern. Supersaturated salt coming out of the glass solution can compromise the integrity of the glass as a permanent nuclear waste storage medium (waste form), increase corrosion in the melter (due to corrosive nature of the molten salt), introduce power instabilities in joule-heated melters, and pose a serious hazard to the melter facility if a continuous layer is formed to short out the electrodes. At the end of the second melter test a total of 4.2 lbs. (1.9 kG) of sodium sulfate ($NaSO_4$) was added to simulate a salt layer in a glass melter [43, 44]. The MMW waveguide was not immersed, but positioned above the melt surface to monitor thermal emission. The dynamics of salt layer formation in a glass melter were observed for the first time. The salt formed small drops first that grew in size until a continuous surface layer was formed. MMW surface fluctuations were coincident with the growth of the molten salt pools on the glass melt.

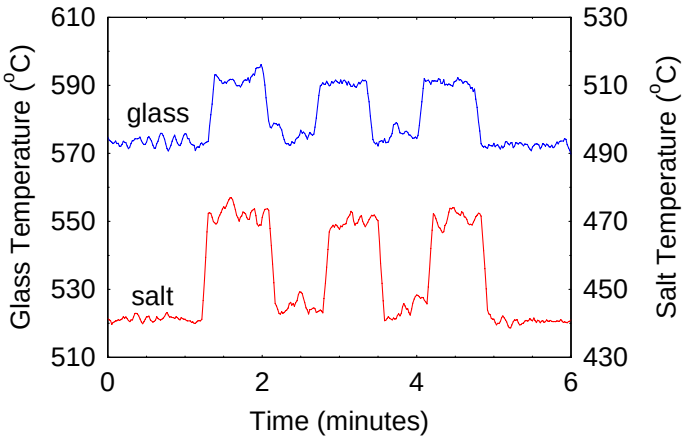

Figure 20. MMW thermal return reflection measurements through an 80% transmitting warm waveguide (~ 360°C) of molten glass and salt at a thermocouple temperature of 950°C.

A quantitative measure of the emissivity of the molten glass and salt at 137 GHz was also obtained with the aid of the TRR

method. Figure 20 shows the TRR data that was recorded. Not only is the MMW temperature of the glass melt higher than the molten salt, but also the ratio of the temperature without to that with the TRR is smaller for the glass melt as expected for a material having a higher emissivity. Using equations 1 - 3 and the thermocouple temperature, the emissivity and surface coupling factor were determined to be: $\varepsilon = 0.64 \pm 0.05$, $\tau_\kappa = 0.46 \pm 0.05$ for the DWPF black frit glass and $\varepsilon = 0.44 \pm 0.05$, $\tau_\kappa = 0.60 \pm 0.05$ for the salt. The MMW emissivity of the molten salt was 32% lower than that for the glass. The difference in coupling factor suggested that the molten salt surface was a smoother, flatter surface (due to its low viscosity hence smooth covering for better return coupling) than the glass melt at these wavelengths.

6.4. Melter Pour Velocity

The capability to measure glass flow velocity in a melter during a pour was demonstrated for the first-time at ACTL [45], as shown in Figure 21 for a SMRF pour of DWPF black glass melt through the bottom spout. The interfreogram shows the receiver video signal, the reflected leaked LO cycling through fringes, as the melt surface drops. The fringes in this case are not rectified as shown in Figures 5 and 13 so counting the positive peaks is equivalent to a surface displacement of ½λ per cycle. Each cycle therefore corresponds to a surface displacement of 1.1 mm for the 137 GHz monitoring frequency. The overall modulation envelope of the fringes is related to the surface receding and changing curvature, which modulates the coupling factor for reflection of the leaked LO back into the waveguide. The dashed curve plots the corresponding surface position showing the surface displacement to be a linear function of time over most of the pour time, corresponding to a constant flow velocity of 0.035 m/s in the pour spout. This is an interesting result since the pressure on the spout from above is a decreasing function of time as the weight of the melt is reduced by the pour, suggesting that the melt may be behaving like a non Newtonian fluid similar to catchup where the viscosity deceases as the pour progresses. Only at the very end of the pour when the melter is almost empty does the flow velocity finally decrease. The viscosity in the pour spout can in principle be determined from this velocity measurement once the instrumentation constant for the pour spout is established. This is similar to viscosity measurement as described above by inducing a pressurized flow in the waveguide, but not exactly the same because the pressure on the spout during the pour is not a constant function of time. However, this data does show that it may possible to check the melt viscosity in the vicinity of the pour spot without immersing the waveguide, but by simply monitoring surface recession rate during a pour, keeping all other parameters constant.

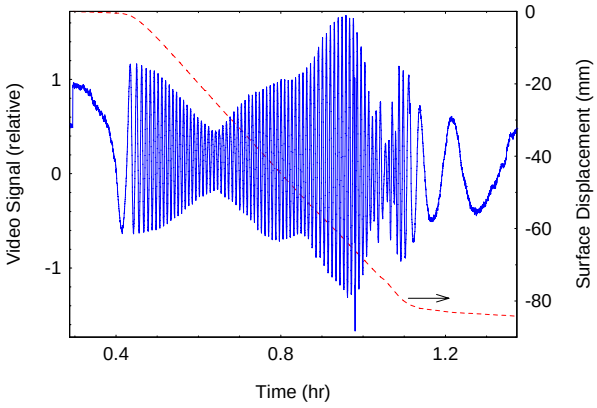

Figure 21. Glass pour interferogram and corresponding surface displacement.

Also interesting new melt pour dynamics are being revealed by this new way of monitoring which may lead to improvements in the way glass is poured.

7. Conclusion

In summary, the main principles of MMW measurements that form the basis of MMW technology for monitoring the vitrification of nuclear wastes have been established. MMWs are ideally suited for monitoring in nuclear waste glass melters because they are tolerant of the imperfections in this environment that would obscure and scatter infrared and optical techniques. The analytical basis, designs, and components of the MMW technology have been outlined for monitoring temperature, emissivity, viscosity, foaming, salt layer formation, and other melter parameters. All of these melter parameters can be monitored simultaneously with a single instrument with only one penetration into the melter of less than 10 cm (2") diameter. Laboratory scale tests and melter measurements have demonstrated and verified the potential of this technology for comprehensive measurements in nuclear waste vitrification facilities. Overall, the MMW technology represents a significant new development for nuclear waste vitrification monitoring that promises to improve the control, efficiency, and reliability for making a high quality nuclear waste glass storage product. It should finally be possible to advance the nuclear waste glass vitrification process to modern industrial standards for feedback control.

References

1. Jantzen, C.M., "Prediction of Glass Durability as a Function of Environmental Conditions", *Proceedings of the Symposium on Materials Stability and Environmental Degradation*, A. Barkatt et. al. (Eds.), Materials Research Society, Pittsburgh, PA, 1988, 143-159.
2. Jantzen, C.M., and Ramsey, W.G., "Prediction of Radioactive Waste Glass Durability by the Hydration Thermodynamic Model: Application to Saturated Repository Environments," *Proceedings of the Symposium on the Scientific Basis for Nuclear Waste Management*, V.M. Oversby and P. Brown (Eds.), Materials Research Society, Pittsburgh, PA, 1990, 217-228.
3. Bickford, D.F., Applewhite-Ramsey, A., Jantzen, C.M., and Brown, K.G., "Control of Radioactive Waste Glass Melters: I, Preliminary General Limits at Savannah River," *J. Am. Ceram. Soc*, 1990, *73* [10] 2896-2902.
4. Andrews, M.K.; Bibler, N.E.; Jantzen, C.M., and Beam, D.C., "Demonstration of DWPF Process and Product Control Strategy by Vitrification of Actual Radioactive Waste," *Proceedings of the 5th International Symposium on Ceramics in Nuclear Waste Management*, G.G. Wicks, D.F. Bickford, and R. Bunnell (Eds.), American Ceramic Society, Westerville, OH, 1991, 569-576.
5. Hutson, N.D.; Jantzen, C.M., and Beam, D.C., "A Pilot Scale Demonstration of the DWPF Process Control Strategy," *Proceedings of the International High-Level Radioactive Waste Management Conference*, Las Vegas, NV, 1992, 525-532.

6. Jantzen, C.M., and Brown, K.G., "Statistical Process Control of Glass Manufactured for the Disposal of Nuclear and Other Wastes," *Am. Ceramic Society Bulletin*, 1993, *72*, 55-59.

7. Cozzi, A.D.; Jantzen, C.M.; Brown, K.G. and Cicero-Herman, C.A., "Process Control for Simultaneous Vitrification of Two Mixed Waste Streams in the Transportable Vitrification System (TVS)," *Environmental Issues and Waste Management Technologies in the Ceramic and Nuclear Industries, Vol. IV Ceramic Transactions*, J. Marra and D.K. Peeler (Eds.), American Ceramic Society, Westerville, OH, (submitted as WSRC-MS-97-00855), 1997.

8. Ryan, J. L., "REDOX Reactions and Foaming in Nuclear Ware Glass Melting," *PNL-10510*, Pacific Northwest Laboratory, Richland, Washington, August 1995.

9. Weinberg, M.C., D. R. Uhlmann, G. L. Smith, "Influence of Radiation and Multivalent Cation Additions on Phase Separation and Crystallization of Glass," *DOE FG07-97-ER45670*, University of Arizona, Tucson, AZ, August 2002.

10. Koopman, D. C.; Lambert, D. P., "Hydrogen Generation and Foaming During Test in the GFPS Simulating DWPF Operations with Tank 42 Sludge and CST," *WSRC-TR-99-00302*, Westinghouse Savannah River Company, Aiken, SC, September 1999.

11. Jantzen, C.M., "DWPF Glass Redox Determination-Summary of Results from Clemson Subcontract," *U.S. DOE Report 86-745*, 1986.

12. Jantzen, C.M., and Plodinec, M.J., "Composition and Redox Control of Waste Glasses- Recommendation for Process Control Limit," *U.S. DOE Report 86-773*, 1986.

13. Calloway, T. B., and Jantzen, C. M., "Analysis of the DWPF Glass Pouring System using Neural Networks(U), *Proceeding of Waste Management 1998*, Tucson, AZ. March 3-4, 1998.

14. Rawlings et. al., "Non-linear Model Predictive Control: A Tutorial and Survey", *Proceedings of ADCHEM '94*, Kyoto, Japan, 1994.

15. Jantzen, C.M. "Characterization of Off-Gas System Pluggages, Significance for DWPF and Suggested Remediation," *U.S. DOE Report WSRC-TR-90-205*, 1991.

16. Jantzen, C.M., "Relationship of Glass Composition to Glass Viscosity, Resistivity, Liquidus Temperature, and Durability: First Principles Process-Product Models for Vitrification of Nuclear Waste," *Proceedings of the 5th International Symposium on Ceramics in Nuclear Waste Management*, G.G. Wicks, D.F. Bickford, and R. Bunnell (Eds.), American Ceramic Society, Westerville, OH, 37-51, 1991.

17. Jantzen, C.M., Pickett, J.B., Brown, K.G., Edwards, T.B., and Beam, D.C., "Process/Product Models for the Defense Waste Processing Facility (DWPF): Part I. Predicting Glass Durability from Composition Using a Thermodynamic Hydration Energy Reaction MOdel (THERMO)," *US DOE Report WSRC-TR-93-0672*, September, 1995.

18. Rivera, D. E.; M. Morari, and S. Skogestead, “Internal Model Control, 4. PIC Controller Design”, *Industrial and Engineering Chemistry Process Design and Development*, Vol. 25, 1986.

19. Cozzi, A.D.; Jantzen, C.M.; Brown K.G., and Cicero-Herman, C.A., “Process Control for Simultaneous Vitrification of Two Mixed Waste Streams in the Transportable Vitrification System (TVS),” *Environmental Issues and Waste Management Technologies in the Ceramic and Nuclear Industries, Vol. IV Ceramic Transactions*, American Ceramic Society, Westerville, OH, 1997.

20. Morari, M., and Zafiriou, E., *Robust Process Control*, Prentice Hall, Engle Cliffs, New Jersey 07632, 1991.

21. Jantzen , C.M., "Prediction of Glass Durability as a Function of Glass Composition and Test Conditions: Thermodynamics and Kinetics", *Proceedings of the First Intl. Conference on Advances in the Fusion of Glass*, American Ceramic Society, Westerville, OH , 1988, 24.1-24.17.

22. Ramsey, W.G., Jantzen, C.M., and Taylor, T.D. “Predictive Modeling of Simulated High-Level Waste Glass pH,” *Proceedings of the 5th International Symposium on Ceramics in Nuclear Waste Management*, G.G. Wicks, D.F. Bickford, and R. Bunnell (Eds.), American Ceramic Society, Westerville, OH, 1991, 105-114.

23. Picton, Phil D. et.al., “Identifying Chemical Species in a Plasma Using Neural Networks”, *Proceedings of the 9th International Conference on Ind. Amd Eng. Application of Artificial Intelligence and Expert Systems*, Fukuoka, Japan, June 4-7, 1996.

24. Shin, Jooho et. al., Design of a Composition Estimator for Inferential Control of High-Purity Distillation Columns”, *Proceedings of the 5th International Conference Chemical Process Control*, 1997, AICHE Symposium Series, *93*.

25. Woskov, P.P.; Sundaram, S. K.; Daniel, G.; Machuzak, J. S.; Thomas, P., “Millimeter-Wave Monitoring of Nuclear Waste Glass Melts – An Overview”, *Environmental Issues and Waste Management Technologies VII*, Ceramic Transactions, 2002, *132*, 189-201.

26. Woskov, P.; Hadidi, K.; Sundaram, S. K., and Daniel, Jr., W. E., “Millimeter-Wave Radiometer Measurement of Emissivity and Temperature by Thermal Return Reflection”, *Inter. Conf. on Infrared and Millimeter-Waves*, San Diego, Sept. 22-26, 2002, *IEEE 02EX561*, 2l1-2l2,.

27. Woskov, P. P.; Cohn, D. R.; Rhee, D. Y.; Thomas, P.; Titus, C. H., and Surma, J. E., “Active Millimeter-Wave Pyrometer”, *Rev. Sci. Instrum.*, 1995, **66**, 4241-4248.

28. Woskov, P.P., and Sundaram, S. K. “Thermal return reflection method for resolving emissivity and temperature in radiometric methods”, *J. Appl. Phys.*, 2002, *92*, 6302-6310.

29. Goldsmith, P. F. *Quasioptical Systems*; IEEE Press, New York, NY 1998; pp. 256-259.

30. Granger, R. A. *Fluid Mechanics*; Dover Publishers, New York, NY 1985;

31. *Haake Viscometers*; Gebrüber HAAKE GmbH, D-7500 Karlsruhe, Germany, 1981.

32. Dicke, R. H., *Rev. Sci. Instr.* 1946, *17*, 268-75.

33. Tiuri, M. E. In *Radio Astronomy*, by J. D. Kraus, Cygnus-Quasar Books, Powell, OH, 1986, Chap. 7.

34. Doane, J. L., "Propagation and Mode Coupling in Corrugated and Smooth-Walled Circular Waveguides", In *Infrared and Millimeter Waves*, Button, K. J., Ed., Academic Press, NY, 1985, Vol. 13, Chap. 5.

35. Marcatili, E. A. J., and Schmeltzer, "Hollow Metallic and Dielectric Waveguides for Long Distance Optical Transmission and Lasers", *The Bell System Technical Journal*, 1964, *43*, 1783-1808.

36. Woskov, P. P., and Titus, C. H., "Graphite Millimeter-Wave Waveguide and Mirror for High Temperature Environments", *IEEE Transactions on Microwave Theory and Techniques*, 1995, *43*, 2684-2688.

37. Woskov P. P.; J. Machuzak, P. Thomas, S. K, Sundaram, and G. Daniel, "High temperature refractory material waveguides for millimeter-wave diagnostics", *Proceedings 10th Intern. Symp. On Laser Aided Plasma Diagnostics*, 6 pages, Fukuoka, Japan, , Sept. 24-28, 2001.

38. Woskov, Paul P.; Bajaj, Vikram S. ; Hornstein, Melissa K.; Temkin, Richard J., and Griffin, Robert G., "Corrugated waveguide and directional coupler for CW 250 GHz gyrotron DNP experiments",*IEEE Trans. of Microwave Theory and Techniques*, 2005, *53*, 1863-1869.

39. Ma, J. Y. L., and Robinson, L. C., " Night moth eye window for the millimetre and sub-millimetre wave region", Optica Acta, 1983, *30*, 1685-1695.

40. Woskov, P. P.; Sundaram, S. K.; Daniel, Jr., W. E., "Waste Glass Melter Process Monitoring with Millimeter Waves", Spectrum 2002, *9th Biennial Conference on Nuclear and Hazardous Waste Management*, American Nuclear Society, Reno, NV, August 4-8, 2002, 5 pages.

41. Woskov, P. P.; Hadidi, K.; Bromberg, L.; Sundaram, S. K.; Rodgers, L. A.; Daniel, Gene, and Miller, Don, "Glass Melt Emissivity, Viscosity, and Foaming Monitoring with Millimeter-Waves", *226th American Chemical Society Meeting CD*, Division of Nuclear Chemistry & Technology, New York, Sept. 7-11, 2003, 81.

42. Sundaram, S. K.; Woskov, P.P.; Machuzak, J.S., and Daniel, Jr., W.E., "Cold Cap Monitoring using Millimeter Wave Technology", In *Environmental Issues and Waste Management Technologies VII*, Editors: G. L. Smith, S. K. Sundaram, and D. R. Spearing, Ceramic Transactions, *132*, 2002, 203-213.

43. Woskov P. P.; Sundaram, S. K.; Daniel, Jr., W. E.; Miller, D.; Harden, J., "Millimeter-wave measurements at137 GHz of DWPF black frit glass flow and salt layer pooling in a pilot scale melter" *227th American Chemical Society Meeting CD*, Division of Environmental Chemistry, March 28 – April 1, 2004, 63, psfc.mit.edu/library/04JA001.

44. Woskov, P. P.; Sundaram, S. K; Daniel, W. E.; Jr., Miller, D., “Molten salt dynamics on glass melt using millimeter-wave emissivity measurements”, *J. of Non Crystalline Solids, 341/1-3,* 2004, 21-25.

45. Woskov, P. P.; Sundaram, S. K; Daniel, W. E.; Jr., Miller, D.,“Millimeter-Wave Measurements of Nuclear Waste Glass Melts”, *Proceedings IRMMW-THZ 2005*, IEEE Cat. No. 05EX1150C, September, 2005, 223-224.